A Computational Approach to Determining the Intrinsic Impedance of Perforated Metal Sheets

by

Erin M. Kiley

A Thesis

Submitted to the Faculty

of the

WORCESTER POLYTECHNIC INSTITUTE

in partial fulfillment of the requirements for the

Degree of Master of Science

in

Applied Mathematics

by

————————————————————

May 2011

APPROVED:

————————————————————

Dr. Vadim V. Yakovlev, Thesis Advisor

————————————————————

Dr. Bogdan Vernescu, Department Head

Abstract

Perforated metal sheets are frequently used in electric and electronic devices, and in most cases, these metal structures should comply with some electromagnetic compatibility constraints which impose certain conditions on penetrating electromagnetic radiation, quality of shielding, and other characteristics. Currently, many issues in electronic system design could be handled with advanced mathematical and computer models; however, direct reproduction of perforation in these models may result in a significantly increased computational cost.

This work is concerned with modeling perforated metal sheets whose apertures have diameters significantly smaller than the wavelength of radiation. We suggest an original approach for computation of intrinsic impedance from the reflection and transmission coefficients obtained by FDTD simulation of the perforated sheet placed in a rectangular waveguide. The calculated impedance can be used to characterize the perforated segment as a solid metal plate which has the same effective material parameters, including electric conductivity.

Functionality of the proposed technique is illustrated with a model of a microwave oven that has two perforated wall segments necessary for ventilation and lighting. After computing the impedance of these segments, they are replaced in the model by solid metal with equivalent effective conductivity, which allows for practical simulation of electromagnetic processes in the oven without any increase in the computational resources required. Computations show that the presence of perforated segments on the walls of this microwave oven makes a negligible impact on the frequency characteristics of the system—so in corresponding full-wave models, the segments can be replaced by solid metal walls without compromising accuracy of simulation.

Acknowledgments

This work was partially sponsored by the EADS Company Foundation, and by General Mills, Inc.

Peter Pesheck and Diane Rosenwald of General Mills were particularly helpful in realizing the need for this work and its potential applications.

Marzena Olszewska of QWED gave useful advice relevant to the computation and verification discussed in Chapter 3.

I give special thanks to my advisor, Prof. Vadim Yakovlev, for the time and energy he has invested in giving me practical insight and guiding me in solving various challenging, interesting problems—and especially for the many useful suggestions he has given in the past few weeks.

For everything in between, I am grateful to my classmates and friends, and most of all, to my parents and to Carlos. It is to them that I dedicate this thesis.

Contents

List of Figures

List of Tables

Abbreviations

EMC	**E**lectro**m**agnetic **C**ompatibility
EMI	**E**lectro**m**agnetic **I**nterference
FDTD	**F**inite **D**ifference **T**ime **D**omain
MW	**M**icro**w**ave
PEC	**P**erfect **E**lectric **C**onductor
QW-3D	**Q**uick**W**ave**-3D**
TE$_{10}$	**T**ransverse **E**lectric **1,0** mode
TEM	**T**ransverse **E**lectro**m**agnetic
UDO	**U**ser-**D**efined **O**bject

Physical Constants

Speed of light in a vacuum	c	$=$	2.99792458×10^8 m/s
Magnetic permeability of free space	μ_0	$=$	$4\pi \times 10^{-7}$ H/m
Electric permittivity of free space	ε_0	$=$	8.8542×10^{-12} farad/m
Intrinsic impedance of free space	η_0	$=$	$\sqrt{\mu_0/\varepsilon_0} = 377 \ \Omega$

Symbols

a	waveguide wide wall	m
d	distance between aperture centers	m
D	aperture diameters	m
k	wavenumber	m^{-1}
R	reflection coefficient of plane wave in a medium	(unitless)
S_{11}	reflection coefficient in waveguide system	(unitless)
S_{21}	transmission loss in waveguide system	(unitless)
t	thickness of metal plate	m
T	transmission coefficient of plane wave in a medium	(unitless)
ε	electric permitivity	F/m
η	electrical impedance	Ω
θ	angle of incidence (in space)	deg
λ	wavelength	m
μ	magnetic permeability	H/m
σ	electric conductivity	S/m
ϕ	angle of incidence (in waveguide)	deg
ω	angular frequency	rad/s

Chapter 1

Introduction

Perforated thin metal plates (see Figure 1.1) have been extensively used in various electric and electronic devices for reduction of weight, cooling, and ventilation. A familiar example of the use of perforation to aid visual monitoring and lighting is in domestic microwave ovens (Figure 1.2), where perforation is used in multiple capacities, appearing as segments of oven walls and in thin layers of metal foil on glass doors.

The development of various technologies has fostered more widespread use of equipment, resulting in an environment increasingly dense with electric and electronic devices [1]. This may allow electromagnetic interference to affect the operation of such equipment, potentially leading to malfunctions. This motivates the application of a variety of standards of electromagnetic compatibility (EMC) which control the level of interference generated by electronic devices. One tool which could assist design engineers in ensuring compliance with increasingly strict standards is advanced mathematical and
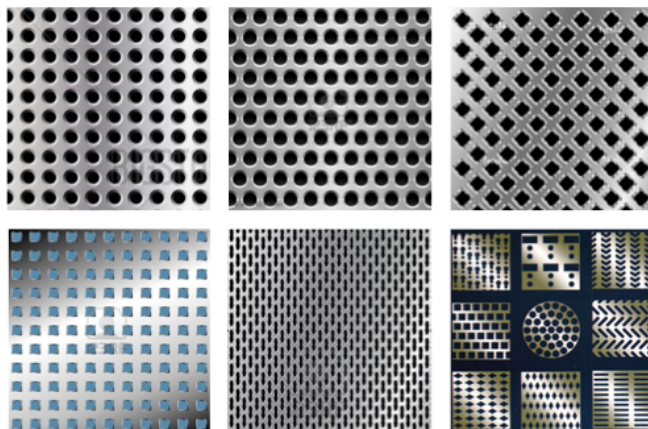
FIGURE 1.1: Examples of perforation pattern in thin metal plates used in various electrical and electronic devices.

(a)	(b)
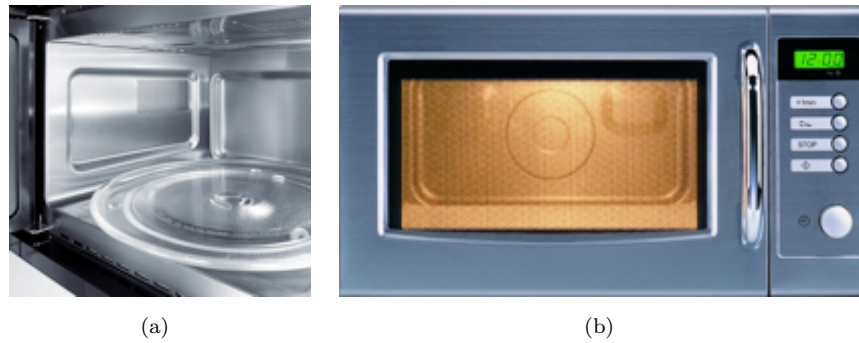
FIGURE 1.2: Examples of metal perforation used on the walls (a) and door (b) of a domestic microwave oven.

computer modeling. As a consequence of this and the prevalence of perforated segments in devices, it is imperative that mathematical and computer models used in design have the ability to accurately describe the effect of perforated metal sheets.

Direct modeling of perforation may be impractical in most EMC scenarios, because characterization of small holes spaced closely together as part of a much larger system would require a mesh so fine in such a large problem, that it would make the model intractable. Modeling techniques based on rigorous explicit [2] and numerical [3] characterization of electromagnetic field scattering on one hole and subsequent integration of the effect of multiple holes have been proposed to analyze wide band transmission and reflection caused by the perforated metal sheets. Special consideration has also been given to narrow band (so-called "extraordinary") transmission through a series of similar holes or slots [4, 5]. These techniques do not, however, provide suitable characterization of perforated metal sheets for full-wave, three-dimensional electromagnetic models representing entire large devices.

Homogenization techniques based on mathematical considerations and physical approximations, including mixture models (e.g., [6–8]), can be viewed as a powerful alternative to the approaches described above; however, similarly, no development of these techniques for characterizing perforated metal sheets by the parameters used in 3D modeling have been reported in literature.

In this project, we suggest a technique applicable to arbitrary perforation comprised by holes or slots smaller than the wavelength of microwave radiation. Our technique is built as a combination of analytical consideration with a numerical model, and is capable of determining the intrinsic impedance η of perforated metal sheets.

Our approach is based on a finite-difference time-domain (FDTD) model determining the reflection (S_{11}) and transmission (S_{21}) coefficients in a section of a rectangular single-mode waveguide containing a perforated metal sheet oriented perpendicularly to the

direction of wave propagation. On the other hand, we deal with a classical two-media model of plane wave propagation leading to a formula expressing the impedance of a lossy medium in terms of the reflection and transmission coefficients R and T.

Because the structure of the plane wave of perpendicular polarization is equivalent to that of the TEM modes into which the considered TE_{10} mode is decomposed, we establish equivalence of R and S_{11}, and T and S_{21}. This leads us to an explicit dependence of the impedance (and thus the electric conductivity σ) of the lossy medium on the reflection and transmission coefficients of the waveguide system, which are determined from the FDTD model. Therefore, when modeling an electromagnetic system with a perforated wall, one can deal, instead of with multiple holes or slots requiring a very fine mesh and increased computational resources, with a solid metal sheet characterized by the effective electric conductivity σ_{eff} found with the use of the proposed computational scheme.

This approach is clearly different from the homogenization techniques, as despite its being associated with the same concept of effective material parameters, it is focused on particular circumstances concerning interaction of perforated metal sheets with the electromagnetic field. On the other hand, the developed approach may recall the principles of FDTD modeling of susceptors [9, 10] whose thickness (usually less than 1 μm) cannot be accounted for with the use of conventional FDTD modeling. These susceptors are replaced in FDTD models by metallic layers of equivalent effective conductivity σ_{eff}, but with greater thickness, making the model more tractable. However, in the referenced papers, σ_{eff} is determined through the resistivity R_s, which is experimentally measured prior to modeling. In this project, we suppose that instrumentation required for measurement of resistivity or conductivity may not be available for engineers designing systems with perforated metal sheets, and with this in mind, we develop a fully computational technique for determination and verification of η, which can be subsequently used to determine σ_{eff}.

We then apply the developed approach to modeling a microwave oven with two segments of perforated wall, as a test of the effect of perforated walls on the frequency response of the reflection coefficient—the characteristic responsible for energy efficiency of microwave heating systems [11, 12]. In the oven studied, the two segments have different spacing between the holes, so we calculate η of each sheet separately, and then replace those segments in FDTD models of the microwave oven by solid metal with equivalent σ_{eff}.

Finally, we simulate the reflection coefficient of the oven with a cylindrical load imitating different food products, and compare the frequency response of the reflection coefficient in this scenario to the response in a separate model, where the perforated segments are replaced by solid metal surfaces that are perfect electric conductors (PEC). The result

of this comparison shows that the perforated segments make a negligible impact, and so they can be replaced in the model by solid PEC segments without compromising the accuracy of the model.

Chapter 2

Theoretical Background

This chapter provides the underlying theory behind our proposed principle of characterizing perforated metal sheets by solid surfaces with equivalent effective electric conductivity (which should be different from the conductivity of PEC). First, we introduce relevant background from the classical problem of propagation of a plane wave near the boundary of two infinite half-spaces, and derive an expression for the impedance of the second medium in terms of the reflection and transmission coefficients of the plane wave. We then describe a numerical model of a single-mode rectangular waveguide containing the perforated metal sheet as a "shorting" wall, introducing an FDTD mesh sufficiently fine to ensure adequate representation of the perforated apertures. Using the decomposition of the structure of an elementary TEM component of the TE_{10} mode and the plane wave of perpendicular polarization, we link the two scenarios and derive an explicit formula expressing the impedance of the perforated sheet as a lossy solid medium in terms of the reflection and transmission coefficients simulated by the waveguide FDTD model.

The key assumption accepted in the proposed computational approach—validity of the two-media model of plane wave propagation when it is used with the parameters of what is naturally a three-media waveguide problem—is then discussed. The approach is made fully rigorous through the introduction of the scenario involving a layer of lossy medium and derivation of the formulas for the reflection and transmission coefficients of the arbitrarily incident plane wave in a three-media model.

2.1 Characterization of Perforated Sheets by Effective Electric Conductivity

Electric conductivity σ is one of the fundamental characteristics of a lossy medium and, as such, is widely used in electromagnetic modeling. It is known to be dependent on the intrinsic impedance η of the medium as follows [13, 14]:

$$\sigma = \left(\frac{1+j}{\eta}\right)^2 \frac{\omega\mu}{2},$$ (2.1)

where $\omega = 2\pi f$, f is the frequency, and μ is permeability, under the condition that the phase angle of the impedance is 45 degrees. This is the case for good conductors, which are the materials considered.

The electromagnetic field in good conductors (such as metals) attenuates very quickly; the skin depth, or characteristic depth of penetration (which indicates the decay of the magnitude of the field in the conductor by an amount of $1/e$ after traveling a distance of δ_s), depends on σ and is defined as

$$\delta_s = \sqrt{\frac{2}{\omega\mu\sigma}}.$$

For example, for such solid metals as aluminum and copper, the skin depth is equal to 8.1×10^{-7} m and 6.6×10^{-7} m respectively [14].

When a thin metal plate contains perforation, propagation of the electromagnetic field through the plate depends on the diameter D of the apertures. If

$$D << \lambda,$$ (2.2)

where $\lambda = c/f$ is the wavelength of the incident plane wave and c is the speed of light, then D is also much smaller than the cutoff wavelength of the aperture when it is considered as a waveguide; as a result, waveguide-type propagation along the perforation holes is not possible. Yet, the electromagnetic field penetrates through the perforated sheet, though undergoing substantial decay in magnitude, which could be considered comparable with attenuation in solid metals.

This consideration implies that thin perforated metal plates could be characterized, in terms of field penetration through them, by some effective electric conductivity σ_{eff}. Furthermore, Formula (2.1) suggests that a perforated sheet in a suitable model can be completely characterized through its impedance. To determine η, we consider propagation of a plane wave through the interface of two semi-infinite media.
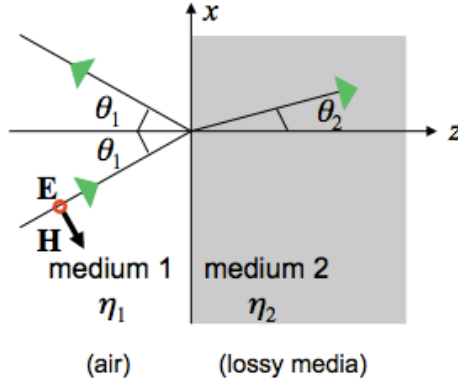
FIGURE 2.1: Plane wave of perpendicular polarization obliquely incident at the interface between two semi-infinite media.

2.2 Impedance of a Lossy Medium in a Two-media Model

The reflection and transmission coefficients R and T for the obliquely incident plane wave hitting the plane interface between two media (Figure 2.1) are introduced here for free space (medium 1) and lossy material (medium 2) [14]:

$$R = \frac{\eta_2 \cos\theta_1 - \eta_1 \cos\theta_2}{\eta_2 \cos\theta_1 + \eta_1 \cos\theta_2}, \quad T = \frac{2\eta_2 \cos\theta_1}{\eta_2 \cos\theta_1 + \eta_1 \cos\theta_2}, \tag{2.3}$$

where θ_1 and θ_2 are the angles of the incident and transmitted waves, respectively. The angle θ_1 in (2.3) can be expressed in terms of θ_2 using Snell's law:

$$\sin\theta_2 = \frac{\eta_2}{\eta_1} \sin\theta_1, \tag{2.4}$$

where η_1 and η_2 are the impedances of free space and the lossy medium, respectively. Combining (2.3) and (2.4), η_2 can be expressed for the plane wave with perpendicular polarization as

$$\eta_2 = \eta_1 \frac{T \cos\theta_2}{T \cos\theta_1 - 2R \cos\theta_1}. \tag{2.5}$$

Since, in accordance with (2.3), the relation between the angles of the incident and transmitted waves is predetermined for the chosen media, we conclude from (2.4) that, for fixed θ_1, determination of the impedance of the lossy media is reduced to finding the reflection and transmission coefficients.
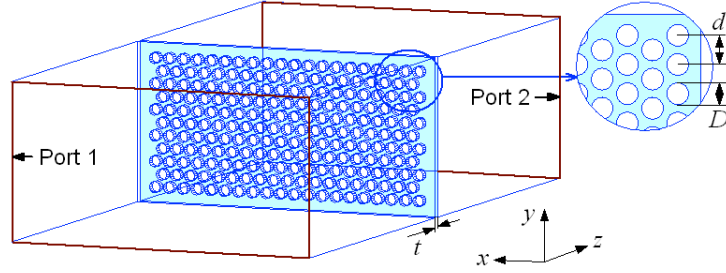
FIGURE 2.2: The concept of an FDTD model simulating reflection and transmission through a perforated metal sheet.

2.3 Impedance as a Function of Waveguide Reflection and Transmission

The above observations suggest the scenario (constructed for a perforated metal plate) in which the angle of the incident wave is known and the reflection and transmission characteristics can be computed numerically. We consider a rectangular waveguide containing a perforated metal sheet oriented perpendicularly to the direction of wave propagation, as shown in Figure 2.2. The wide wall of the waveguide a is chosen to guarantee a single-mode regime and ensure condition (2.2). With the use of an appropriate numerical technique applied over a sufficiently small mesh discretizing the perforation, one can compute the reflection and transmission coefficients (S_{11} and S_{21}) of the system in Ports 1 and 2 respectively.

We consider decomposition of the dominant TE_{10} mode into the sum of two TEM waves propagating at the speed of light at oblique angles ϕ with respect to the z-axis (Figure 2.3) [13, 15]. The x-component of the velocity vector of the TEM wave is shown in Figure 2.4. The superposition of the two waves along the x-axis produces a standing wave between the narrow walls of the waveguide, and the phase velocity in this direction is given by

$$v_x = \frac{2ac}{\lambda},$$

and thus the angle ϕ can be determined from

$$\sin \phi = \frac{\lambda}{2a}. \tag{2.6}$$

Since the orientation of the field components of the TEM modes is identical to the orientation of the components of the plane wave with perpendicular polarization, the angle of the incident wave θ_1 in (2.5) can be considered equal to the angle ϕ associated
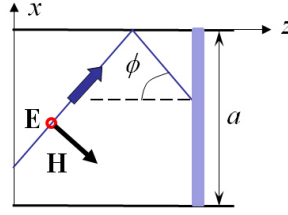
FIGURE 2.3: A partial TEM mode in a rectangular waveguide.
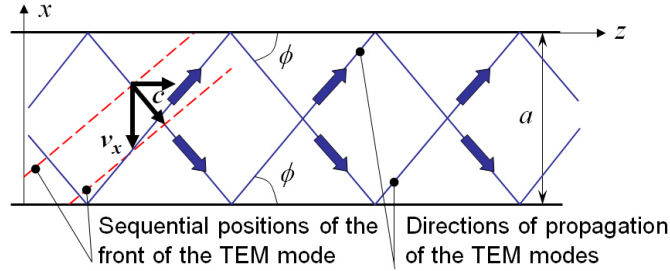
FIGURE 2.4: TE$_{10}$ mode decomposed into two TEM modes.

with waveguide propagation of the TEM modes:

$$\theta_1 = \phi. \tag{2.7}$$

Therefore, combination of (2.6) with (2.4) yields

$$\cos\theta_1 = \sqrt{1 - \left(\frac{\lambda}{2a}\right)^2} \quad \text{and} \quad \cos\theta_2 = \sqrt{1 - \left(\frac{\eta_2}{\eta_1}\right)^2 \left(\frac{\lambda}{2a}\right)^2}. \tag{2.8}$$

In the numerical model of the considered waveguide system, S_{21} is determined in the port positioned on the far side of the perforated sheet in air. However, because of the inevitable substantial attenuation of the electromagnetic field penetrating through the perforated sheet, we assume that the influence of the second interface (medium-air) can be ignored, and thus the computed S_{21} is identical to the one determined in the medium (prior to that interface—similar to the two-media scenario considered in Section 2.2). This leads to equivalence of the reflection and transmission characteristics in the waveguide model and in the two-media consideration of the plane wave.

Substitution of (2.8) into (2.5) and interpretation of R and T as S_{11} and S_{21} respectively leads to a formula for the intrinsic impedance η of the perforated metal sheet,

$$\eta = \frac{\eta_1 S_{21}}{\sqrt{(S_{21} - 2S_{11})^2 + S_{11}S_{21}\left(\frac{\lambda}{a}\right)^2 - (S_{11})^2\left(\frac{\lambda}{a}\right)^2}}, \tag{2.9}$$
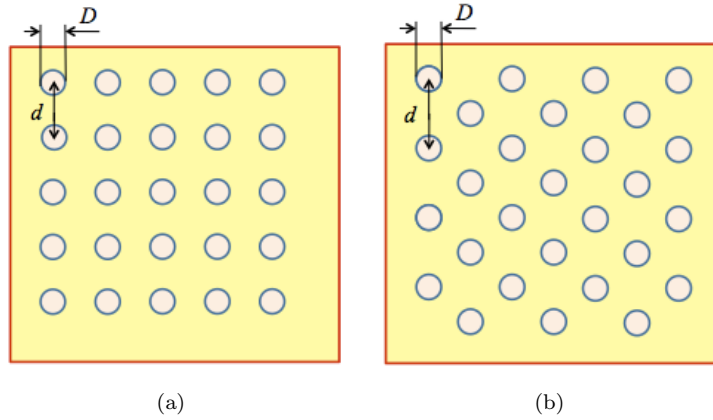
FIGURE 2.5: Square (a) and equilateral triangular (b) lattices of circular apertures in perforated sheets.

in terms of S_{11} and S_{21} determined through numerical modeling of the waveguide scenario. Effective conductivity of the perforated sheet can then be computed with the use of (2.1). The Matlab code carrying out the corresponding computation is presented in Appendix A.1.

2.4 Numerical Modeling of a Waveguide Scenario

The proposed computational approach to finding the intrinsic impedance of perforated metal sheets combines analytical consideration with numerical modeling needed for determination of waveguide reflection and transmission. With numerical simulation used as a part of the technique, this approach is independent of the geometrical characteristics of perforation, and is thus applicable to various patterns of holes and slots (for example, any of those shown in Figure 1.1).

In this work, we consider two patterns of perforation apertures which are popular in practice—those of square and equilateral triangular lattices of circular holes (with inter-hole spacing d and hole diameter D) shown in Figure 2.5. To ensure high accuracy of numerical simulation with minimal computational resources, we use a 3D conformal FDTD technique which has proven very efficient in modeling electrically large structure with small geometrical elements [16–19].

Geometry of the FDTD-simulated waveguide scenario is shown in Figure 2.2. In accordance with FDTD principles, to ensure adequacy and accuracy of computation, the model is meshed with sufficiently small cells (chosen so that the cell size is sufficiently smaller than λ, and so that it is in accordance with the Courant stability criterion—that is, the number of cells should be consistent with the size of the time step, which should

not be too small in order to control the number of iterations needed). A suitable mesh should have cells in the x- and y-directions small enough to ensure accurate geometrical representation of the circular apertures. In the model, the system is excited by a pulse of spectrum, and simulations are run until the energy in the system dissipates to a sufficiently low level.

Use of this FDTD model in determination of η also provides a convenient mechanism for verification of the output of the proposed computational technique. In this verification, the values of S_{11} and S_{21} obtained from the model of the waveguide scenario (Figure 2.2) are compared with S_{11} and S_{21} resulting from a similar model in which the perforated sheet is replaced by a solid plate characterized by σ_{eff} computed from (2.1) and (2.9).

2.5 Impedance of a Lossy Medium in a Three-media Model

As mentioned in Section 2.3, the considered computational approach operates under the assumption that, due to the substantial attenuation of the field penetrating through the perforation in a thin metal plate, the second interface in the direction of waveguide propagation (the medium-air interface in Figure 2.2) makes an insignificant impact on the value of S_{21} and this characteristic can thus be considered identical with T of a plane wave in the two-media consideration (Figure 2.1). Since this assumption is induced from a rather qualitative assessment, here we consider the waveguide scenario in combination with a more general three-media (air-medium-air) model for the plane wave and evaluate the conditions of its reduction to the two-media analysis.

For the case of a three-media model of an obliquely incident plane wave and a thin layer sandwiched between two semi-infinite spaces occupied by the same medium (Figure 2.6), the reflection and transmission coefficients R and T can be expressed on the basis of the related analysis in [20]:

$$R = \frac{\eta_2^2 - \eta_1^2}{\eta_2^2 + \eta_1^2 + 2i\eta_2\eta_1 \cot(k_{2z}t)}, \qquad T = \frac{2\eta_1\eta_2}{\eta_2^2 + \eta_1^2 + 2i\eta_2\eta_1 \cot(k_{2z}t)}, \qquad (2.10)$$

where t is the thickness of medium 2, $k_{2z} = k_2 \cos\theta_2$, and k_2 is the wavenumber in medium 2.

Rearrangement of the formulas in (2.10) results in the following relation:

$$\eta_2^2 - \eta_1^2 = \frac{2iR\eta_1\eta_2}{T\sin(k_{2z}t)},$$

and η_2 can thus be found from the quadratic equation
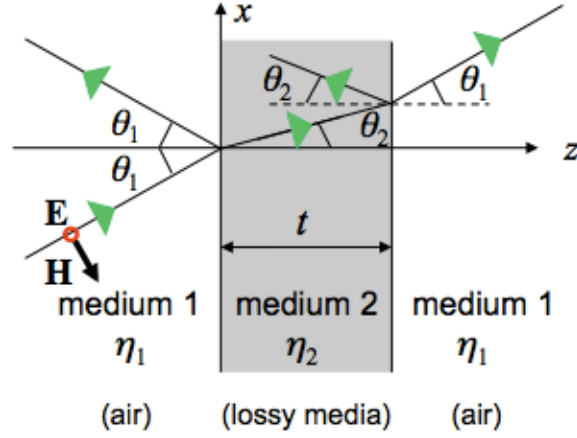
FIGURE 2.6: Plane wave of perpendicular polarization obliquely incident at the surface of a lossy medium of finite thickness.

$$\eta_2^2 - \eta_2 \left[2i \frac{R}{T} \eta_1 \csc(k_2 t \cos \theta_2) \right] - \eta_1^2 = 0. \tag{2.11}$$

From (2.6) and Snell's law (2.4), we obtain that

$$\cos \theta_2 = \sqrt{1 - \left(\frac{\lambda \eta_2}{2a\eta_1} \right)^2}. \tag{2.12}$$

Substituting (2.12) into (2.11) and replacing R and T by S_{11} and S_{21}, the equivalents of reflection and transmission in a waveguide respectively, we obtain

$$\eta_2^2 - \eta_1^2 - \frac{2i\eta_1\eta_2 S_{11}}{S_{21} \sin \left[k_2 t \sqrt{1 - \left(\frac{\lambda \eta_2}{2a\eta_1} \right)^2} \right]} = 0. \tag{2.13}$$

Note that the right-hand side of (2.13) is a nonlinear function of η_2, and as such, we would like to use numerical solvers to find its roots. Special attention must be paid, however, to the fact that it is a complex function of a complex variable, and in order to be differentiable as such, it must satisfy the Cauchy-Riemann conditions. As shown in Appendix B, the function does not, in fact, satisfy these conditions, and so numerical methods relying on the derivative cannot be considered accurate for this scenario.

Despite the fact that (2.13) has not been used as an analytical verification of the impedance resulting from (2.9), this equation is still valuable as a theoretical part of the model resulting in a complete computational technique.

Chapter 3

Computational Implementation

Here we outline important details of the computational realization of the technique described in the previous chapter. First, we review key parameters of the considered waveguide scenario, its corresponding FDTD model, and required computational resources. Illustrative computations of the reflection and transmission coefficients in the waveguide system are then validated by a separate FDTD model, in which a perforated sheet is replaced by a solid plate with effective conductivity equivalent to that of the perforated plate.

3.1   Waveguide Scenario and Computational Details

We apply the computational technique of Chapter 2 to determine the impedance and the effective electric conductivity of perforated metal sheets with square and equilateral triangular lattices of circular apertures (Figure 2.5). With particular interest in results obtained at the frequency $f = 2.45$ GHz, and with an obligation to satisfy condition (2.2), we study sheets with $1 \leq t \leq 4$ mm, $1 \leq D \leq 4$ mm, and $1 \leq d \leq 3$ mm, choosing a rectangular waveguide with relevant cross-sectional dimensions of 86×43 mm.

The numerical model of the waveguide scenario is constructed for the 3D conformal FDTD simulator *QuickWave-3D*, ver. 7.5 (*QW-3D*) [21]. The code used to characterize the geometry of systems containing plates with square and triangular lattices of circular apertures are shown in the *QW-3D* UDO files in Appendices C.1 and C.2 respectively. The waveguide structure is meshed in accordance with the conditions described in Section 2.4, with 20 cells per wavelength, so that the total number of cells in the project is approximately 300,000, both for the case of a triangular lattice and for the case of a square lattice. An example of a suitable nonuniform mesh (with larger cells in the

(a)

(b)
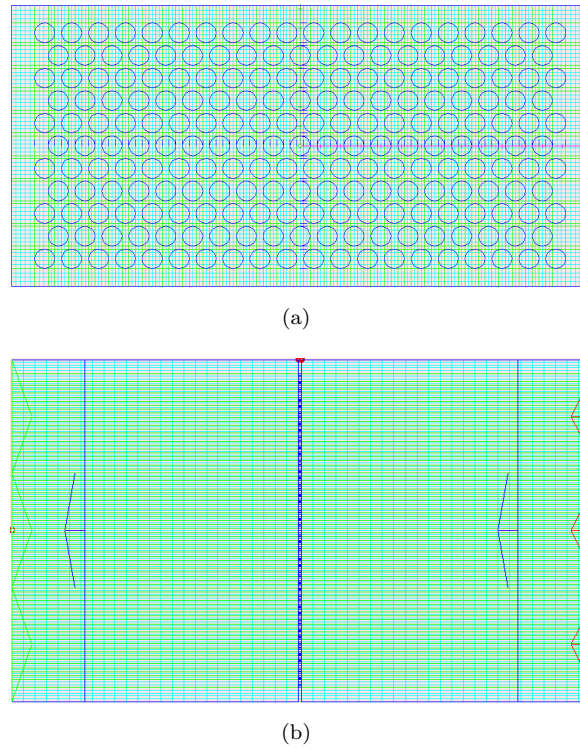
FIGURE 3.1: The xy-plane (a) and xz-plane (b) views of an FDTD mesh in a waveguide scenario.

TABLE 3.1: Computational Results for the Perforated Sheet with Equilateral Triangular Lattice ($d = 4$ mm)

D, mm	t, mm	$|S_{11}|$	$< S_{11}, °$	$|S_{21}|$	$< S_{21}, °$	σ_{eff}, S/m
3.0	2.0	0.9999	-94.49	0.0005	178.6	9.2×10^5
	1.0	0.9999	-94.57	0.0013	177.0	1.7×10^5
3.6	2.0	0.9999	-94.04	0.0007	179.0	4.9×10^5
	1.0	0.9962	-95.31	0.0015	176.6	1.2×10^5

z-direction and smaller cells in the x- and y-directions) adequate to ensure accurate geometrical representation of circular apertures in perforation is shown in Figure 3.1. To ensure high accuracy of computation, FDTD simulations using this model were run until they reached steady state, determined by monitoring the energy in the system, which was expected to dissipate to the level of 10^{-9}–10^{-10} [nJ].

Since all types of modeling projects involving perforated metal sheets are computationally expensive, the computations were performed using an OMP version of the multithread implementation of the *QW-3D* simulator found particularly efficient in accelerating FDTD computations. Simulations were run on a Dell T-4700 workstation (64-bit Windows XP) with 16 GB of RAM and two quad-core Intel Xeon 3.20 GHz processors. The entire procedure was hastened using the Acceleware A30 card (NVIDIA Quadro

TABLE 3.2: Verification of the Computed σ_{eff} (2.45 GHz, $d = 4$ mm, $t = 1$ mm)

	$D = 3.0$ mm		$D = 3.6$ mm	
Waveguide model	$|S_{11}|$	$< S_{11}$	$|S_{11}|$	$< S_{11}$
Perforated Sheet	0.9999	-94.57	0.9962	-95.31
Solid Plate with Equivalent σ_{eff}	0.9991	-94.26	0.9995	-94.24

FX 5600) implementing GPU technology in the form of integrated FDTD hardware accelerators.

Typical results of computations aiming to determine η and σ_{eff} of perforated metal sheets are presented in Table 3.1, which also includes the magnitude and phase of complex reflection and transmission coefficients. The results make sense from a physical viewpoint: transmission through the perforated sheets becomes higher for larger D, smaller d, and smaller t, and the same trend is observed for effective conductivity. For $t \gtrsim 2$ mm, the values of $|S_{11}|$ and $|S_{21}|$ are so close to 1 and 0 respectively, that they are identical to the fourth significant digit, which seems to correspond to the conditions in which propagation through the perforated sheet becomes too weak due to the large thickness of the metal plate. The situations in which $|S_{11}| \to 1$ and $|S_{21}| \to 0$ may be therefore considered a computational limit of the presented technique and its implementation.

3.2 Numerical Validation of the Technique

Computational output of the developed technique can be verified using a similar model in which the perforated sheet is replaced by a solid plate with the computed σ_{eff} (Table 3.2). It can be seen that the results obtained by both of the models are close, which confirms our computational approach as a technique sufficiently accurate to be used in practice.

We also perform here a special, qualitative validation of the physical concept in the background of the developed technique, carried out by numerical computation of the electric field pattern in the waveguide with a thin perforated metal plate. The field patterns in this structure are shown in Figure 3.2 in all three coordinate planes. More specifically, patterns (a) and (b) display the field in the center slices on the xz- and yz-planes respectively. Column (c) shows the field patterns in selected slices of the xy-planes in the segment adjacent to Port 1 and in four successive layers of the FDTD cells around the perforated sheet—counting downward (from Port 1 to Port 2), two layers prior to the sheet, one layer through the sheet and two layers after the sheet. The slices are scaled independently of one another, and the magnitude of the field at the central point of each xy-pattern is provided. The field of the TE_{10} mode is
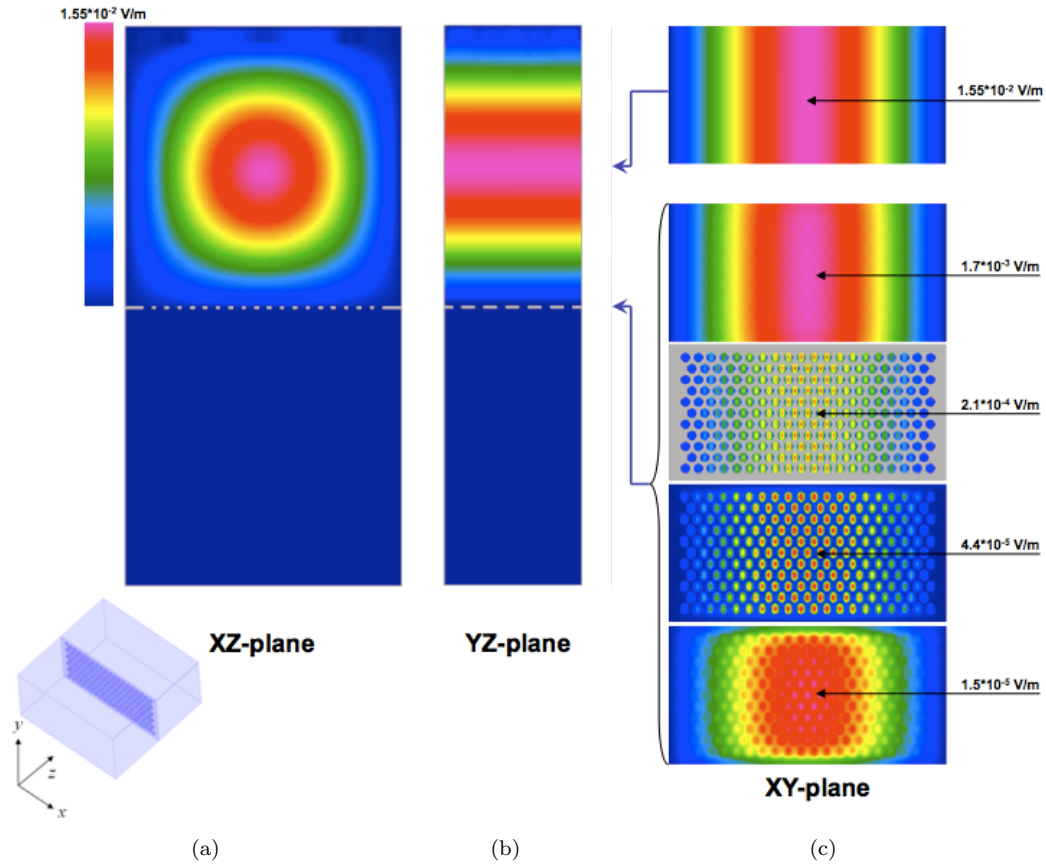
FIGURE 3.2: Electric field patterns in the rectangular waveguide containing a thin metal sheet.

clearly visible in the waveguide segment adjacent to Port 1, whereas the field on the other side of the perforated sheet is characterized by a very low magnitude, with the structure of the TE_{10} mode destroyed. When passing through the perforated sheet, the field substantially decays. This qualitatively confirms the principles of the developed technique relying on computation of both S_{11} and S_{21} and assuming strong attenuation of the field penetrating through the small apertures in the perforation.

Finally, it is worth mentioning that in the particular case of a normally incident wave, analytical formulas exist for the reflection and transmission coefficients of a perforated metal sheet with circular (or square) apertures, which depend only on the geometrical characteristics of the sheet and the waveguide [2]. However, these formulas are not applicable to our results, as our computational model considers the more general case of oblique incidence.

Chapter 4

A Practical Computational Example

The technique outlined in Chapter 2 and tested and verified in Chapter 3 has been applied to check for the effect of perforated walls on the frequency response of the reflection coefficient in the 600 W *Sanyo Direct Access* (Figure 4.1), a domestic microwave oven with two segments of perforation on its metal walls.

4.1 Modeling the *Sanyo Direct Access* MW Oven

All important details of the geometrical configuration of the *Sanyo Direct Access* oven are shown in Figure 4.2. The cavity measures $a \times b \times c = 290 \times 300 \times 185$ mm, operates at 2.45 GHz, and is excited by a waveguide ($g_a \times g_b = 86 \times 43$ mm), located at $s = 35$ mm and $p = 152$ mm from the cavity's edges. The oven is modeled with a cylindrical

FIGURE 4.1: The *Sanyo Direct Access* microwave oven.
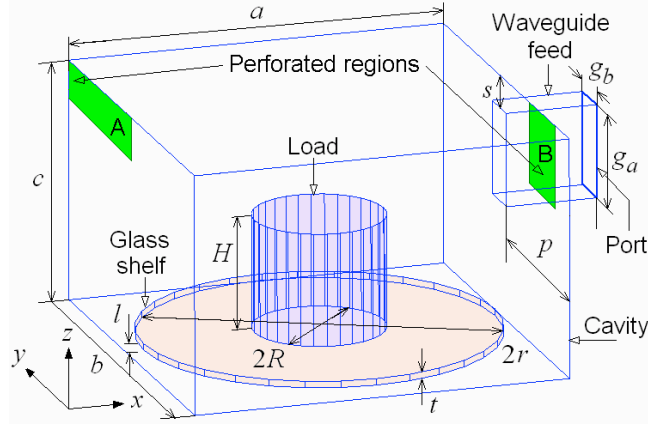
FIGURE 4.2: Geometrical characterization of the *Sanyo Direct Access* microwave oven, with perforated wall segments A and B.
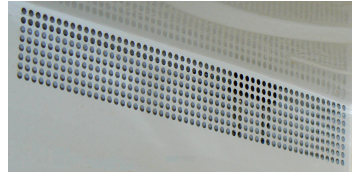
FIGURE 4.3: Perforated segment A (Figure 4.2) in the *Sanyo Direct Access* microwave oven.

TABLE 4.1: Dielectric Properties of the Loads (2.45 GHz, 20°C) [22].

Food product	Dielectric constant ε'	Conductivity σ (S/m)
Water	78.7	1.465
White bread	4.14	0.211
Corn oil	2.63	0.020

0.1 l load ($R = 25$ mm, $H = 51$ mm) placed on the center of a turntable (a cylindrical disk of $r = 136$ mm and $t = 5$ mm) at a height of $l = 5$ mm from the bottom.

Simulations are performed for three food products (Table 4.1) very different in their dielectric properties, and with glass ($\varepsilon' = 6.0$, $\sigma = 0$) as the medium of the turntable. The oven contains two perforated wall segments, each having a square lattice of circular apertures: A (220×35 mm) with $D = 3.0$ mm and $d = 4.0$ mm, and B (60×80 mm) with $D = 3.6$ mm and $d = 4.0$ mm. Segment A is shown in Figure 4.3.

In the FDTD model developed for the entire system, the space inside the resonant cavity and waveguide is discretized with a non-uniform mesh (the maximum cell sizes are 6 mm in air, 3.5 mm in glass, 4 mm in corn oil, 3.5 mm in white bread, and 1.2 mm in water) with approximately 365,000 to 1,072,000 cells, depending on the type of load. Code characterizing the geometry of the oven is shown in the *QW-3D* UDO file in Appendix
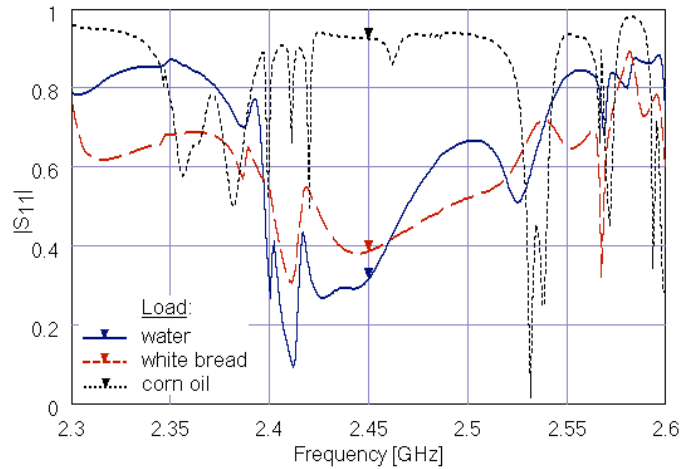
FIGURE 4.4: Frequency response characteristics of the magnitude of reflection coefficient in the *Sanyo Direct Access* microwave oven loaded with different food products; each curve represents two characteristics–first, with segments A and B taken to be PEC, and second with A and B taken to be solid metal surfaces characterized by σ_{eff}.

C.3. FDTD simulation using this model reaches steady state in about 120,000 (corn oil) to 230,000 (water) iterations, so a single computation takes from 22 to 90 min.

4.2 Calculating Impedance of Perforated Segments

Simulations performed using the technique described in Chapter 3 show that the values of the effective conductivity of segments A and B are 1.2×10^5 and 1.7×10^5 S/m respectively. These values are used to characterize the solid metal surfaces which replace segments A and B. FDTD simulation is subsequently run on the entire microwave oven after replacing A and B by these surfaces and by PEC, with the resulting frequency response of the reflection coefficient described in the following section.

4.3 FDTD Modeling Results

Our simulations (Figure 4.4) show that the frequency characteristics of the microwave oven, loaded with any of the three materials considered, before and after replacing the perforated segments A and B by solid segments with corresponding σ_{eff} for each region, are indistinguishable. This provides a direct answer to an important practical question—whether the presence of perforated segments of microwave oven walls should be taken into account when modeling electromagnetic processes occurring in the system. Our results demonstrate that the perforated segments do not have any visible influence on

(a)

(b)
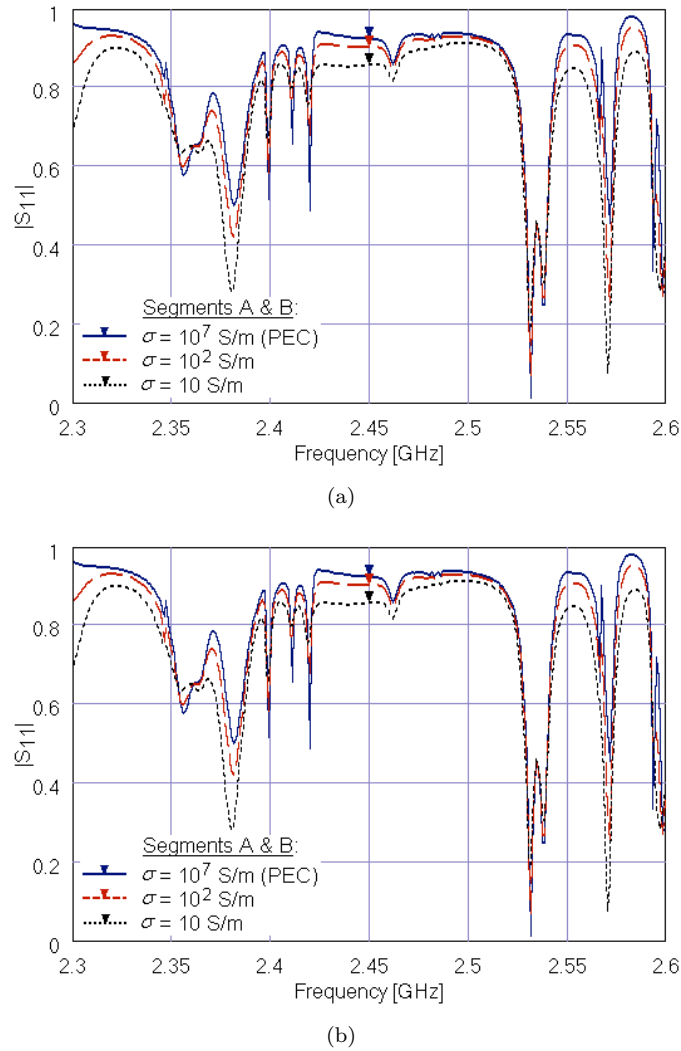
FIGURE 4.5: The reflection coefficient in the *Sanyo Direct Access* microwave oven for different effective conductivity of Segments A and B; loads are water (a) and corn oil (b).

the frequency responses of the reflection coefficients—the characteristics responsible for the energy efficiency of microwave ovens [11, 12].

As seen from the curves in Figure 4.5, a notable effect from perforation in segments A and B occurs only when σ_{eff} is artificially decreased by 4-5 orders of magnitude. However, these levels of effective conductivity are attainable only with geometrical characteristics of perforations which appear impractical for microwave ovens. It therefore may not be an exaggeration to state that when modeling microwave ovens, any relatively small perforated wall regions could be safely considered as solid PEC segments. These results do not, however, preclude a more significant effect from larger regions of perforation in different systems, such as resonant cavities with the walls made entirely of perforated metal sheets.

Chapter 5

Conclusions

This work has devised and implemented an original computational technique for determining the intrinsic impedance of perforated metal sheets used in many applied electric and electronic devices. The technique relies on an FDTD model of a single-mode, rectangular waveguide containing a perforated metal sheet oriented perpendicularly to the direction of field propagation. Analytical formulas for the impedance have been derived from the established equivalence of the reflection and transmission coefficients in the waveguide with the reflection and transmission coefficients characterizing propagation of a plane wave through the interface of two semi-infinite media. A more general scenario associated with propagation of a plane wave in a three-media model has also been considered. It has been suggested that, in numerical models describing systems involving thin perforated metal segments, the segments could be replaced by solid metal surfaces characterized by effective conductivity determined from the formula for the intrinsic impedance.

The developed technique has been implemented as a battery of computer codes in *QuickWave-3D*, Matlab, and Maple, and has been used for computation of impedance and effective conductivity of perforated sheets with square and equilateral triangular lattices of circular apertures—two commonly used structures of perforated segments in devices. The computational output has been verified by a similar FDTD model of the waveguide structure containing a solid metal plate with the determined effective conductivity, which has allowed us to estimate the limits of the constructed computer implementation.

Computational tests have been performed to study the influence of perforation in the walls of a particular microwave oven on the characteristics responsible for its operating efficiency. In a special FDTD model developed for the *Sanyo Direct Access* microwave oven, small perforated metal wall segments were replaced by solid PEC sheets, and

it has been demonstrated that this replacement does not compromise accuracy of the simulation. It has therefore been concluded that in corresponding numerical models, typically small perforated segments in the walls of microwave ovens can be ignored.

The proposed technique can also be used for characterization of perforated metal sheets and screens employed in various practical pieces of equipment to address related EMC problems.

Future work may include an analytical validation of the two-layer model via reduction from a three-layer or multi-layer model, and implementation of the algorithm on a more advanced (in terms of productivity) hardware, allowing for quicker computation of the model with finer a FDTD mesh, which may extend the computational limits of the current version. The sensitivity of the frequency response of the reflection coefficient to the size of the region of perforation may also be studied.

Appendix A

MATLAB Codes

A.1 Calculation of Electric Conductivity from Known Reflection and Transmission: Two-Media Model

```
1  function [eta,sigma]=conduct2(a,lambda,omega,mu,R,T,p)
2  % function [eta,sigma]=conduct2(a,lambda,omega,mu,R,T,p)
3  %
4  % Calculates the electric conductivity of a metal sheet given its
5  % transmission and reflection characteristics. Uses the two-layer
      model.
6  %
7  % Inputs: a - position of waveguide wall
8  %         lambda - wavelength
9  %         omega - angular frequency
10 %         mu - permeability
11 %         R - reflection coefficient (S11)
12 %         T - transmission coefficient (S21)
13 %         p - p is 1 for parallel polarization, 0 for
      perpendicular
14 % Outputs: sigma - electric conductivity
15 %          eta - electric impedance
16
17 eta1=377; %impedance of free space (ohms)
18
19 if p==1 %parallel polarization
20     c4=-0.25*(lambda*lambda/a*a*eta1*eta1);
21     c3=0;
22     c2=T*T-4*R*R*(1-0.25*(lambda*lambda/(a*a)));
23     c1=-4*R*T*(1-0.25*(lambda*lambda/(a*a)));
```

```matlab
24        c0 =0;
25
26        etavals=roots([c4 c3 c2 c1 c0]); %impedance is root of a
        quartic polynomial
27        fprintf('Four possible impedances found: %g, %g, %g, and %g\n'
        ,etavals(1), etavals(2), etavals(3), etavals(4));
28        etacoord=50;
29        while etacoord~=1 && etacoord~=2 && etacoord~=3 && etacoord~=4
30        etacoord=input('Please enter 1, 2, 3, or 4 to use the
        corresponding above impedance value.\n>');
31        end
32        eta=etavals(etacoord);
33
34 elseif p==0 %perpendicular polarization
35        eta=eta1*T/sqrt((T-2*R)*(T-2*R)+...
36            (R*T*(lambda*lambda/(a*a)))-(R*R*lambda*lambda/(a*a))); %
        impedance
37 %      fprintf('Two possible impedances found: %g or %g\n',eta,-eta)
        ;
38 %      posneg=50;
39 %      while posneg~=1 && posneg~=2
40 %      posneg=input('Please enter 1 or 2 to use the corresponding
        above impedance value.\n>');
41 %      end
42
43 %      if posneg==2
44 %          eta=-eta;
45 %      end
46
47 else %huh?
48        error('p should be 0 or 1');
49 end
50
51 %fprintf('eta=%s\n',num2str(eta));
52 sigma=0.5*(omega*mu)*((1+1j)*(1+1j)/(eta*eta));
53 %fprintf('sigma=%s\n',num2str(sigma));
54
55 sigma=abs(sigma);
56
57 end
```

Appendix B

Maple Worksheet

B.1 The Three-Media Function and the Cauchy-Riemann Condition

The three-media model is described by the formula

$$f := z \rightarrow z^2 - p^2 - \frac{z \cdot 2 \cdot I \cdot R \cdot p}{T \cdot \sin\left(k \cdot t \cdot \mathrm{sqrt}\left(1 - \left(\frac{l \cdot z}{2 \cdot a \cdot p}\right)^2\right)\right)};$$

$$z \rightarrow z^2 - p^2 - \frac{2\,\mathrm{I}\,z\,R\,p}{T \sin\left(k\,t\,\sqrt{1 - \frac{1}{4}\frac{l^2 z^2}{a^2 p^2}}\right)} \tag{1}$$

where p is impedance of free space, t is the thickness of the plate, a is the length of the waveguide in the direction of propagation, l is the wavelength, k is the wavenumber in the sheet, and R and T are the reflection and transmission coefficients in the waveguide.

Note that we are solving for the complex impedance $z := x + I \cdot y$ which gives $f(z) = 0$. To do this using an iterative method such as Newton's or the Broyden update, we need to differentiate f; that is, we should find its Jacobian. In order that this is a valid derivative, we must confirm that the Cauchy-Riemann conditions are satisfied; that is, we need $u_x = v_y$ and $u_y = -v_x$, where u and v are the real and imagnary parts, respectively, of $f(x, y)$. We carry out the following calculations to see whether the first condition holds:

$$g := (x, y) \rightarrow f(x + I \cdot y);$$
$$(x, y) \rightarrow f(x + \mathrm{I}\,y) \tag{2}$$
$$u := (x, y) \rightarrow evalc(\mathrm{Re}(g(x, y)));$$
$$(x, y) \rightarrow evalc(\Re(g(x, y))) \tag{3}$$
$$v := (x, y) \rightarrow evalc(\mathrm{Im}(g(x, y)));$$
$$(x, y) \rightarrow evalc(\Im(g(x, y))) \tag{4}$$
$$evalb(\mathit{diff}(u(x, y), x) - \mathit{diff}(v(x, y), y) = 0);$$
$$\mathit{false} \tag{5}$$

So the first Cauchy-Riemann condition does not, in fact, hold.

Appendix C

QW-3D UDO Scripts

C.1 Model of a Waveguide Containing a Sheet with a Square Lattice of Circular Holes

```
1  name="square";
2  comment="Test system; holes in square arrangement";
3  bitmap="square.bmp";
4
5  PAR("object name",oname,"testsystem");
6  PAR("cavity medium",cavitymed,metal);
7  PAR("cavity height (x-dir)",cavityx,30);
8  PAR("cavity width (y-dir)",cavityy,50);
9  PAR("cavity length (z-dir)",cavityz,200);
10
11 PAR("distance of holey wall from input port (z-dir)",wallportz
      ,100);
12 PAR("thickness of holey wall (z-dir)",wallz,2);
13
14 PAR("diameter of holes",holediam,2);
15 PAR("distance between hole centers (y-dir)",holespacey,3);
16 PAR("distance between hole centers (x-dir)",holespacex,3);
17
18 PAR("Maximum cell size in x-dir",cx,4);
19 PAR("Maximum cell size in y-dir",cy,4);
20 PAR("Maximum cell size in z-dir",cz,4);
21
22 PAR("Maximum cell size in x-dir within mesh restricted zone",sx,1)
      ;
23 PAR("Maximum cell size in y-dir within mesh restricted zone",sy,1)
      ;
```

```
24  PAR("Maximum cell size in z-dir within mesh restricted zone",sz,1)
        ;
25
26  ENDHEADER;
27  OPENOBJECT(oname);
28
29  TEST(holespacex>holediam,"Spacing must be greater than diameter");
30  TEST(holespacey>holediam,"Spacing must be greater than diameter");
31  TEST(wallportz+wallz<cavityz,"Wall distance must be smaller than
        cavity length");
32
33  #draw cavity
34  CALL("elements/cubic.udo",cavity,cavityx,cavityy,cavityz,cavitymed
        ,x,y,z,9);
35  #draw wall
36  CALL("elements/cubic.udo",wall,cavityx,cavityy,wallz,cavitymed,x,y
        ,z+cavityz-wallportz-wallz,9);
37
38  #cut holes from wall
39  dx=holespacex;
40  dy=holespacey;
41  r=holediam/2;
42  ly=cavityy;
43  lx=cavityx;
44
45  fy=dy+2*r;
46  ny=((ly-fy)/(dy))+1;
47  ay=0.5*(ly-2*r-(int(ny)-1)*dy);
48
49  fx=dx+2*r;
50  nx=((lx-fx)/(dx))+1;
51  ax=0.5*(lx-2*r-(int(nx)-1)*dx);
52
53  i=1;
54  while i<=int(nx) do
55      j=1;
56      while j<=int(ny) do
57      holename=("hole"@STR(i)@"and"@STR(j));
58      CALL("elements/cyv.udo",holename,r,wallz,16,air,E,x-0.5*cavityx
        +ax+r+(i-1)*dx,y-0.5*cavityy+ay+r+(j-1)*dy,z+cavityz-wallportz-
        wallz,10);
59  #    MARK(ELEM,ALL,RESET);
60  #    MARKFJ(ELEM,wall,PASSIVE);
61  #    MARKFJ(ELEM,holename,ACTIVE);
```

```
62 #    JOIN(CUT);
63 #    MARK(ELEM,ALL,RESET);
64    j=j+1;
65    endwhile;
66 #x-snapping planes
67 CALL("elements/specx.udo",spx@STR(i)@top,1,x-0.5*cavityx+ax+2*r+(i
      -1)*dx,y,z,6);
68 CALL("elements/specx.udo",spx@STR(i)@bot,1,x-0.5*cavityx+ax+(i-1)*
      dx,y,z,6);
69 i=i+1;
70 endwhile;
71
72 #y-snapping planes
73 j=0;
74 while j<=ny do
75 CALL("elements/specy.udo",spy@STR(i)@top,1,x,y-0.5*cavityy+ay+2*r
      +(j-1)*dy,z,6);
76 CALL("elements/specy.udo",spy@STR(i)@top,1,x,y-0.5*cavityy+ay+(j
      -1)*dy,z,6);
77 j=j+1;
78 endwhile
79
80
81
82 #port
83 CALL("elements/portz.udo",port,cavityx,cavityy,DOWN,1,3,NO,x,y,z+
      cavityz,11);
84
85 #MESHPAR(cx,cy,cz,0,0,0,0,0,0,1);
86 MESHPAR(sx,sy,sz,x-0.5*cavityx,x+0.5*cavityx,y-0.5*cavityy,y+0.5*
      cavityy,z+cavityz-wallportz-wallz,z+cavityz-wallportz,1);
87 CLOSEOBJ;
```

C.2   Model of a Waveguide Containing a Sheet with a Triangular Lattice of Circular Holes

```
 1  name="triangular";
 2  comment="Test system; holes in equitriangular arrangement";
 3  bitmap="triangular.bmp";
 4
 5  PAR("object name",oname,"testsystem");
 6  PAR("cavity height (x-dir)",cavityx,86);
 7  PAR("cavity width (y-dir)",cavityy,43);
 8  PAR("cavity length (z-dir)",cavityz,174.4);
 9
10  PAR("distance of holey wall from input port (z-dir)",wallportz
        ,87.2);
11  PAR("thickness of holey wall (z-dir)",wallz,2);
12
13  PAR("diameter of holes",holediam,2.5);
14  PAR("distance between hole centers (x-dir)",dx,4);
15
16  #PAR("Maximum cell size in x-dir",cx,4);
17  #PAR("Maximum cell size in y-dir",cy,4);
18  #PAR("Maximum cell size in z-dir",cz,4);
19
20  PAR("Maximum cell size in x-dir within mesh restricted zone",sx,1)
        ;
21  PAR("Maximum cell size in y-dir within mesh restricted zone",sy,1)
        ;
22  PAR("Maximum cell size in z-dir within mesh restricted zone",sz,1)
        ;
23
24  ENDHEADER;
25  OPENOBJECT(oname);
26
27  TEST(dx>holediam,"Spacing must be greater than diameter");
28  TEST(wallportz+wallz<cavityz,"Wall distance must be smaller than
        cavity length");
29
30  #draw cavity
31  CALL("elements/cubic.udo",cavitybot,cavityx,cavityy,cavityz-
        wallportz-wallz,air,x,y,z,9);
32  CALL("elements/cubic.udo",cavitytop,cavityx,cavityy,wallportz,air,
        x,y,z+cavityz-wallportz,9);
33
```

```
34  #cut holes from wall
35  r=holediam/2;
36  dy=0.5*dx*sqrt(3);
37
38  nx=(1/dx)*(cavityx-2*r-dx)+1;
39  ax=0.5*(cavityx-2*r-dx*(int(nx)-1));
40
41  ny=(1/dy)*(cavityy-2*r-dy)+1;
42  ay=0.5*(cavityy-2*r-dy*(int(ny)-1));
43
44  zpos=z+cavityz-wallportz-wallz;
45  i=1;
46  offrow=0;
47  while i<=ny do
48      j=1;
49      ypos=y-0.5*cavityy+ay+r+(i-1)*dy;
50      while j<=(nx-offrow) do
51      holename=("hole"@STR(i)@"and"@STR(j));
52      CALL("elements/cyv.udo",holename,r,wallz,16,air,E,x-0.5*cavityx
        +ax+r+(j-1)*dx+offrow*0.5*dx,ypos,zpos,10);
53  #    MARK(ELEM,ALL,RESET);
54  #    MARKFJ(ELEM,wall,PASSIVE);
55  #    MARKFJ(ELEM,holename,ACTIVE);
56  #    JOIN(CUT);
57  #    MARK(ELEM,ALL,RESET);
58      j=j+1;
59      endwhile;
60  offrow=1-offrow;
61  #y-snapping planes
62  CALL("elements/specy.udo",spy@STR(i)@top,1,x,ypos+r,z,6);
63  CALL("elements/specy.udo",spy@STR(i)@bot,1,x,ypos-r,z,6);
64  i=i+1;
65  endwhile;
66
67  #x-snapping planes
68  j=1;
69  while j<=nx-1 do
70      CALL("elements/specx.udo",spx@STR(j)@top,1,x-0.5*cavityx+ax+2*r
        +(j-1)*dx,y,z,6);
71      CALL("elements/specx.udo",spx@STR(j)@bot,1,x-0.5*cavityx+ax+(j
        -1)*dx,y,z,6);
72      CALL("elements/specx.udo",spx@STR(j)@offsettop,1,x-0.5*cavityx+
        ax+2*r+(j-1)*dx+0.5*dx,y,z,6);
```

```
73      CALL("elements/specx.udo",spx@STR(j)@offsetbot,1,x-0.5*cavityx+
        ax+(j-1)*dx+0.5*dx,y,z,6);
74      j=j+1;
75  endwhile;
76  CALL("elements/specx.udo",spx@STR(int(nx))@top,1,x-0.5*cavityx+ax
        +2*r+(int(nx)-1)*dx,y,z,6);
77  CALL("elements/specx.udo",spx@STR(int(nx))@bot,1,x-0.5*cavityx+ax
        +(int(nx)-1)*dx,y,z,6);
78
79  #ports 1 & 2
80  CALL("elements/portz.udo",portin,cavityx,cavityy,DOWN,1,22,
        portpulse,x,y,z+cavityz,11);
81  CALL("elements/portz.udo",portout,cavityx,cavityy,UP,2,22,
        portpulse,x,y,z,11);
82
83  #MESHPAR(cx,cy,cz,0,0,0,0,0,0,1);
84  MESHPAR(sx,sy,sz,x-0.5*cavityx,x+0.5*cavityx,y-0.5*cavityy,y+0.5*
        cavityy,z+cavityz-wallportz-wallz,z+cavityz-wallportz,1);
```

C.3 Model of the *Sanyo Direct Access* Microwave Oven

```
 1 comment="Sanyo Direct Access microwave oven peroforated walls
       segments";
 2 bitmap="mwoven.bmp";
 3
 4 PAR( "Object name", onam, ovenh );
 5
 6 PAR( "Oven x-dim", ol, 290 );
 7 PAR( "Oven y-dim", ow, 300 );
 8 PAR( "Oven z-dim", oh, 185 );
 9
10 PAR( "Feeding waveguide x-dim", fwl, 70 );
11 PAR( "Feeding waveguide y-dim", fww, 34 );
12 PAR( "Feeding waveguide z-dim", fwh, 72 );
13 PAR( "Feeding waveguide z-position (from bottom)", fwz, 88 );
14 PAR( "Feeding waveguide y-position (from centre)", fwy, -17 );
15
16 PAR( "Patch A x-dim", pal, 12 );
17 PAR( "Patch A y-dim", paw, 220 );
18 PAR( "Patch A z-dim", pah, 35 );
19
20 PAR( "Patch B x-dim", pbl, 12 );
21 PAR( "Patch B y-dim", pbw, 60 );
22 PAR( "Patch B z-dim", pbh, 80 );
23 PAR( "Patch B y-position", pby, 30);
24
25 #PAR( "Load x-dim", lx, 100 );
26 #PAR( "Load y-dim", ly, 70 );
27 #PAR( "Load z-dim", lz, 30 );
28
29 PAR( "Cyl. load: radius", lr, 25 );
30 PAR( "Cyl. load: height", lh, 51 );
31
32 PAR( "Load z-position", lp, 10 );
33 PAR( "Load shift from ctr in x-dir", sx, 0 );
34 PAR( "Load shift from ctr in y-dir", sy, 0 );
35
36 PAR( "Shelf diameter", sd, 272 );
37 PAR( "Shelf height (z-dir)", sh, 5 );
38 PAR( "Shelf z-position", sz, 5 );
39
40 PAR( "Shelf medium", smed, TTglass );
41 PAR( "Load medium", lmed, water2450 );
```

```
42  PAR( "Patch A medium", pamed, conduct130 );
43  PAR( "Patch B medium", pbmed, conduct136 );
44
45  PAR( "Mesh in air", amesh, 6);
46  PAR( "Mesh in load", lmesh, 1.2);
47  PAR( "Mesh in shelf", smesh, 3.5);
48
49  ENDHEADER;
50
51  TEST( oh>0, "Oven height should be greater than 0" );
52  TEST( ol>0, "Oven length should be greater than 0" );
53  TEST( ow>0, "Oven width should be greater than 0" );
54
55  TEST( fwh>0, "Feeding waveguide height should be greater than 0" )
        ;
56  TEST( fwl>0, "Feeding waveguide length should be greater than 0" )
        ;
57  TEST( fww>0, "Feeding waveguide width should be greater than 0" );
58  TEST( fwz<=oh-fwh&&fwz>=0, "Feeding waveguide should be inside the
         oven" );
59  TEST( fwy<=ow/2-fww/2&&fwy>=-ow/2+fww/2, "Feeding waveguide should
         be inside the oven" );
60
61  TEST( sd>0, "Shelf diameter should be greater than 0" );
62  TEST( sh>0, "Shelf height should be greater than 0" );
63  TEST( sz>0, "Shelf z-position should be greater than 0" );
64
65  OPENOBJECT(onam);
66
67  # Draw the oven
68  CALL( "elements/cubic.udo", box, ol, ow, oh, air, x, y, z, 9 );
69
70  # Draw the patches of "perforation"
71  # Patch A - on the wall opposite waveguide
72  CALL( "elements/cubic.udo", patcha, pal, paw, pah, pamed, x+0.5*ol
        +0.5*pal, y-0.5*ow+0.5*paw, z+oh-pah, 9 );
73
74  # Patch B - on the wall alongside the waveguide
75  CALL( "elements/cubic.udo", patchb, pbl, pbw, pbh, pbmed, x-0.5*ol
        -0.5*pbl, y+0.5*ow-pby-0.5*pbw, z+oh-pbh, 9 );
76
77  # Joining elements
78  MARKFJ( ELEM, box, PASSIVE );
79  MARKFJ( ELEM, patcha, ACTIVE );
```

```
 80  MARKFJ( ELEM, patcha, ACTIVE );
 81  JOIN( CUT );
 82
 83  # Draw the feeding waveguide
 84  CALL( "elements/cubic.udo", onam@fw, fwl, fww, fwh, air, x-ol/2-
        fwl/2, y+fwy, z+fwz, 9 );
 85
 86  # Draw the shelf
 87  CALL( "elements/cyv.udo", onam@shelf, sd/2, sh, 32, smed, E, x, y,
        z+sz, 10 );
 88
 89  # Draw the load - rectangular block
 90  # CALL( "elements/cubic.udo", onam@load, lx, ly, lz, meat, x+sx, y
        +sy, z+lp, 9 );
 91
 92  # Draw the load - cylinder
 93  CALL( "elements/cyv.udo", onam@cload, lr, lh, 32, lmed, E, x, y, z
        +sz+sh, 10 );
 94
 95  # Global mesh - cell sizes in x-, y-, z-directions
 96  MESHPAR( amesh, amesh, amesh, 1, 2, 1, 2, 1, 2, 1 );
 97
 98  #Draw SPs
 99  CALL( "elements/specx.udo", spyx, 2, x-ol/2, y, z, 6 );
100  CALL( "elements/specy.udo", spy1, 2, x, y-0.5*ow+paw, z, 6 );
101  CALL( "elements/specy.udo", spy2, 2, x, y+0.5*ow-pby, z, 6 );
102  CALL( "elements/specy.udo", spy3, 2, x, y+0.5*ow-pby-pbw, z, 6 );
103
104  CALL( "elements/specxu.udo", onspxu1", 2, lmesh, x-lr+sx, y, z, 7)
        ;
105  CALL( "elements/specxd.udo", onspxd1", 2, lmesh, x+lr+sx, y, z, 7)
        ;
106  CALL( "elements/specyu.udo", onspyu1", 2, lmesh, x, y-lr+sy, z, 7)
        ;
107  CALL( "elements/specyd.udo", onspyd1", 2, lmesh, x, y+lr+sy, z, 7)
        ;
108
109  CALL( "elements/specxu.udo", onspxu2", 2, smesh, x-sd/2, y, z, 7);
110  CALL( "elements/specxd.udo", onspxd2", 2, smesh, x-lr+sx, y, z, 7)
        ;
111  CALL( "elements/specxu.udo", onspxu3", 2, smesh, x+lr+sx, y, z, 7)
        ;
112  CALL( "elements/specxd.udo", onspxd3", 2, smesh, x+sd/2, y, z, 7);
113
```

```
114  CALL( "elements/specyu.udo", onspyu2", 2, smesh, x, y-sd/2, z, 7);
115  CALL( "elements/specyd.udo", onspyd2", 2, smesh, x, y-lr+sy, z, 7)
        ;
116  CALL( "elements/specyu.udo", onspyu3", 2, smesh, x, y+lr+sy, z, 7)
        ;
117  CALL( "elements/specyd.udo", onspyd3", 2, smesh, x, y+sd/2, z, 7);
118
119  CALL( "elements/speczu.udo", onspzu1", 2, lmesh, x, y, z+sz+sh, 7)
        ;
120  CALL( "elements/speczd.udo", onspzd1", 2, lmesh, x, y, z+sz+sh+lh,
        7);
121  CALL( "elements/speczd.udo", onspzd2", 2, 2.5, x, y, z+sz+sh, 7);
122
123  # Draw port
124  CALL( "elements/portx.udo", onam@port, fwh, fww, "UP", 1, fwl/2,
        ovenhport, x-ol/2-fwl, y-fww/2+fwy, z+fwz, 11 );
125
126  CLOSEOBJ;
```

Bibliography

[1] H. Ott, *Electromagnetic Compatibility Engineering.* New York: J. Wiley & Sons, 2009.

[2] C. Chen, "Transmission of microwave through perforated flat plates of finite thickness," *IEEE Trans. Microwave Theory & Techniques*, vol. MTT-21, no. 1, pp. 1–6, 1973.

[3] N. Doncov, A. Wlodarczyk, R. Scaramuzza, and V. Trenkic, "TLM modeling of perforated thin metal screens," 4th Intern. Conf. on Computation in Electromagnetics, 2002.

[4] V. Lomakin, N. Chen, S. Li, and E. Michielssen, "Enhanced transmission through two-period arrays of sub-wavelength holes," *IEEE Microwave and Wireless Components Letters*, vol. 14, no. 7, pp. 355–357, 2004.

[5] F. Medina, F. Mesa, and R. Marques, "Equivalent circuit model to explain extraordinary transmission," in *IEEE MTT-S Int. Microw. Symp. Dig.*, (Atlanta, GA), pp. 213–216, June 2008.

[6] C. Brosseau and A. Beroual, "Computational electromagnetics and the rational design of new dielectric heterostructures," *Progress in Materials Science*, vol. 48, pp. 373–456, 2003.

[7] K. Whites, "Effects of particle shape on the effective permittivity of composite materials with measurements for lattices of cubes," *IEEE Trans. on Microwave Theory and Techniques*, vol. 50, pp. 1723–1729, July 2002.

[8] F. Wu and K. Whites, "Quasi-static effective permittivity of periodic composites containing complex shaped dielectric particles," *IEEE Trans. on Antennas and Propagation*, vol. 49, August 2001.

[9] M. Celuch, W. Gwarek, and M. Soltysiak, "Effective modeling of microwave heating scenarios including susceptors," in *Recent Advances in Microwave Theory & Appl. (Microwave-2008)*, (Jaipur, India), pp. 404–405, November 2008.

[10] W. Gwarek, M. Celuch, and J. Krupka, "Modeling and measurements of susceptors for microwave heating applications," in *2009 IEEE MTT-S Int. Microwave Symp. Workshop "Recent Advances in Microwave Power Applications & Techniques" (RAMPAnT)*, (Boston, MA, USA), June 2009.

[11] T. Koutchma and V. Yakovlev, *Computer Modeling of Microwave Heating Processes for Food Preservation*, ch. Mathematical Analysis of Food Processing, pp. 625–657. CRC Press, 2010.

[12] M. Celuch and P. Kopyt, *Modeling Microwave Heating in Foods*, ch. Development of Packaging and Products for Use in Microwave Ovens, pp. 305–348. Oxford: Woodhead Publishing, 2009.

[13] R. Collin, *Foundations for Microwave Engineering*. New York: IEEE Press, 2 ed., 2001.

[14] D. Pozar, *Microwave Engineering*. New York: J. Wiley & Sons, 2005.

[15] R. Sarbacher and W. Edson, *Hyper and Ultrahigh Frequency Engineering*. New York: J. Wiley & Sons, 1943.

[16] A. Taflove and S. Hagness, *Computational Electrodynamics: the Finite-Difference Time-Domain Method*. Boston - London: Artech House, 3 ed., 2005.

[17] W. Yu, X. Yang, Y. Liu, R. Mittra, and A. Muto, *Advanced FDTD Methods: Parallelization, Acceleration, and Engineering Applications*. Boston - London: Artech House, 2011.

[18] J. D.G. Swanson and W. Hoefer, *Microwave Circuit Modeling Using Electromagnetic Field Simulation*. Boston - London: Artech House, 2003.

[19] M. Celuch and W. Gwarek, "Properties of the FDTD method relevant to the analysis of microwave power problems," *J. Microwave Power & Electromag. Energy*, vol. 41, no. 4, pp. 62–80, 2007.

[20] L. Brekhovskikh, *Waves in Layered Media*. London: Academic Press, 1980.

[21] QuickWave-3D. QWED Sp., z.o.o, Warsaw, Poland, 1988–2008. http://www.qwed.com.pl.

[22] P. Risman, *Microwave Dielectric Properties of Foods and Some Other Substances*, ch. Development of Packaging and Products for Use in Microwave Ovens, pp. 153–175. Oxford: Woodhead Publishing, 2009.